CLM-P824

Tokamak division contributions to 14th European Conference on controlled fusion and plasma physics (Madrid, 22-26 June 1987)

UK ATOMIC ENERGY AUTHORITY

Culham Laboratory

CLM-P824

Tokamak division contributions to 14th european conference on controlled fusion and plasma physics (Madrid, 22-26 June 1987)

Culham Laboratory, Abingdon, Oxon, OX14 3DB, UK
(UKAEA/Euratom Fusion Association)

October 1987

Tokamak Division contributions to 14th European Conference on Controlled Fusion and Plasma Physics (Madrid, 22-26 June 1987).

ECRH PROGRAMME WITH HIGH-FIELD-SIDE LAUNCH ON DITE TOKAMAK

M.W. Alcock, N.R.G. Ainsworth, P.R. Collins, M. Cox, A.N. Dellis, S.J. Fielding, J. Hugill, I. Johnson, P.C. Johnson, B. Lloyd, C. Moeller*, M. O'Brien, R. Prater*, A.C. Riviere, D.C. Robinson, A. Simonetto+ and T.N. Todd

UKAEA Culham Laboratory/Euratom Association, Abingdon, Oxon OX14 3DB, U.K.
*G.A. Technologies Inc., PO Box 85608, San Diego, California 92138, USA.
+Attached under a Euratom Scholarship

INTRODUCTION

DITE tokamak has been modified to allow electron cyclotron resonance heating using three 60GHz, 200kW Varian gyrotrons with power launched from the high field side of the torus. To make space for the antennae the major radius has been increased by 20mm resulting in the following parameters: R_o = 1.19m, a = 0.24m, B_T < 2.7T, I_p = 173kA (at B_T = 2.15T, q=3). Typical target plasmas in D_2 or He have $T_{eo} \approx 0.8 \pm 0.2$keV, $\bar{n}_e = 0.5\text{-}10 \times 10^{19} m^{-3}$.

Two types of antenna are being used, as illustrated in Fig.1. Type A has a water-free, fused quartz window between the launch point and the region where electron cyclotron resonance occurs in the feed waveguide, which carries the HE_{11} mode and is filled with dry nitrogen at atmospheric pressure. A grooved, rotatable mirror directs radiation from the antenna aperture, which is 200mm above the median plane, towards the magnetic axis. This mirror is designed to convert the linearly polarised wave radiated by the antenna to an elliptically polarised wave which closely matches the X-mode in the plasma. Thus we expect a high fraction of the radiated power to couple to the X-mode.

The type B antenna has a remote vacuum window, so that the waveguide is evacuated in the region of cyclotron resonance. To avoid breakdown in this region, the waveguide which carries the TE_{11} mode is split in two longitudinally. A bias of up to 2kV can be applied between the two halves [1]. The grooved mirror, positioned close to the median plane in this case, directs the radiated power horizontally.

At present two type A and one type B antennae are installed each fed from a distance of about 50m by a gyrotron with a power greater than 200kW. The transmission lines [2] involve conversion from the TE_{02} gyrotron output mode to the low-loss TE_{01} mode for the main waveguide run and then to HE_{11} (TE_{11}) mode for the type A (B) antennae. Calorimetrically measured losses in the transmission lines are ~10%.

THEORETICAL HEATING AND CURRENT DRIVE PROFILES

The propagation and absorption of the radiated power as a function of launch angle, ϕ and toroidal field have been calculated using a ray-tracing

method. Plasma density and temperature profiles are represented by $n_e = n_{eo}(1 - r^2/a^2)^{0.7}$ and $T_e = T_{eo}(1 - r^2/a^2)^2$ respectively. A conical bundle of 45 rays with 10° half angle represents the radiation pattern of the antennae.

Power deposition profiles for $n_{eo} = 4\times10^{19}m^{-3}$ and $B_T = 2.14T$, giving $\omega = \omega_{ce}$ on axis, are shown in Fig.2 for various launch angles. The region of maximum absorption moves away from the axis as ϕ increases mainly due to refraction effects. At ϕ=45° the absorption efficiency is 100%, decreasing at higher values of n_{eo} because of the reduction in T_e at the absorption zone and hence in the number of electrons available for Doppler resonance.

As the cyclotron layer is moved outwards by increasing B_T, Doppler resonance can occur in the hotter central regions. This is illustrated in Fig.3 for which $\omega = \omega_{ce}$ at r/a = 0.5. Reasonably high current drive efficiencies are possible because the absorption occurs at high $k_\parallel$ in the plasma centre. For example, with $\omega = \omega_{ce}$ at $R_o + 3a/4$, $n_e(o) = 2\times10^{19}m^{-3}$, $T_e(o)$ = 3keV the current drive efficiency is predicted to be ~ 0.3A/W (neglecting electron trapping effects).

As expected, the maximum density which can be accessed is somewhat less than the X-mode cut-off density of $8.8\times10^{19}m^{-3}$ because of refraction. However, some experiments (DIII, FT1) have been able to achieve significant heating at densities well above cut-off in the plasma centre. One of our aims is to explore this phenomenon further.

EXPERIMENTAL RESULTS

Experiments with toroidal field only used 100kW, 100ms pulses from one type A and one type B antenna with ω/ω_{ce}=1 at $R_o - a/2 < R < R_o$. At D_2 filling pressures of $\sim10^{-4}$mB, plasmas of density $\overline{n}_e \sim 4\times10^{18}m^{-3}$ could be sustained during the microwave pulse. Such plasmas are of interest for tokamak start up, to reduce the transformer flux consumed during the initial phase of the discharge. Using the type B antenna, a discharge occurs in the evacuated waveguide when a resonance is present and the bias is not applied. This is strongly absorbing, so that the gyrotron continues to operate consistently at 130kW for 100ms. For technical reasons, the bias has not yet been applied.

Initial experiments in deuterium target plasmas used $B_{To} = 2.14T$ (central resonance) $I_p \sim 100kA$, $T_e(o) \simeq 800eV$ and a_L restricted to 0.21m to avoid possible antenna damage due to disruptions. Plasmas with densities, $\overline{n}_e = 10^{19}m^{-3}$ up to the density limit at $4\times10^{19}m^{-3}$ were heated by 100ms ECRH pulses from one type A antenna at a power level of 100 to 150kW. Fig.4 shows traces of the main discharge parameters in a typical shot. During ECRH there is an increase in plasma energy and a decrease in loop voltage whose time dependence indicate an absorbed power of ~ 80kW. The small

density increase is typical but dependent on the condition of the vacuum wall. The increase in total radiation is less than 20kW. The changes in plasma energy and loop voltage during ECRH (Fig.5) are insensitive to $\bar{n}_e$, where the highest density ($\bar{n}_e = 4\times10^{19}m^{-3}$) corresponds to ~70% of X-mode cut-off. Small Marfes observed near the density limit were not strongly affected by ECRH and did not appear to reduce the heating efficiency.

These preliminary results indicate good access to high density plasma with high field side launch of ECRH power.

ACKNOWLEDGEMENTS

This work was partially funded by the U.S. Department of Energy.

DITE tokamak operations were supervised by R.W. Storey. Messrs M. Dunstan, B.J. Parham, J. Pritchard and J.P. Webber provided invaluable experimental assistance. Gyrotron operations were supported by Messrs S.R.C. Green, D. Moody, J. Riley and S. Goodenough.

REFERENCES

[1] C. Moeller, G.A. Technologies Report No. GA-A 18836.

[2] A.N. Dellis, N.R.G. Ainsworth, P.R. Collins, D. Moody and J.S. Trigg. Eleventh International Conference on Infrared and Millimeter Waves, Tirrenia, Pisa (1986). Conference Digest p.314.

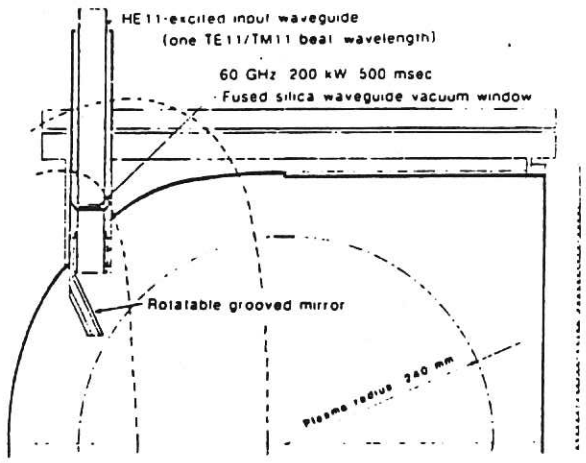

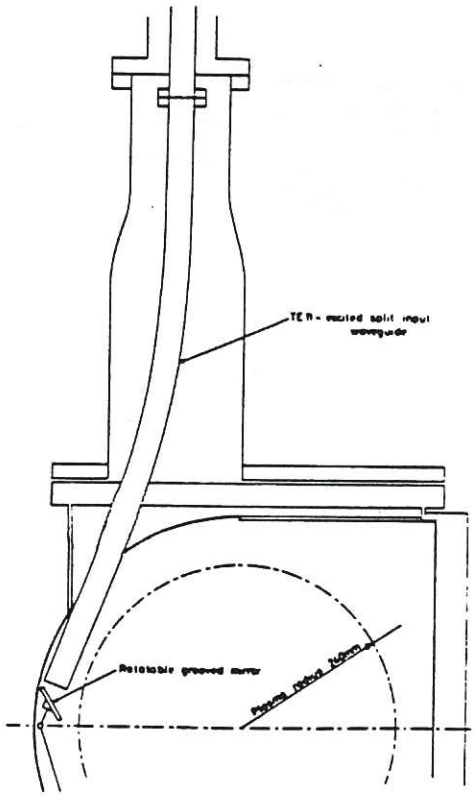

Fig.1 Above: Type A antenna with fused quartz window. The waveguide has dry nitrogen at atmospheric pressure in the region of cyclotron resonance.
Right: Type B antenna with remote vacuum window. The waveguide is split and biassed to avoid breakdown in the region of cyclotron resonance.

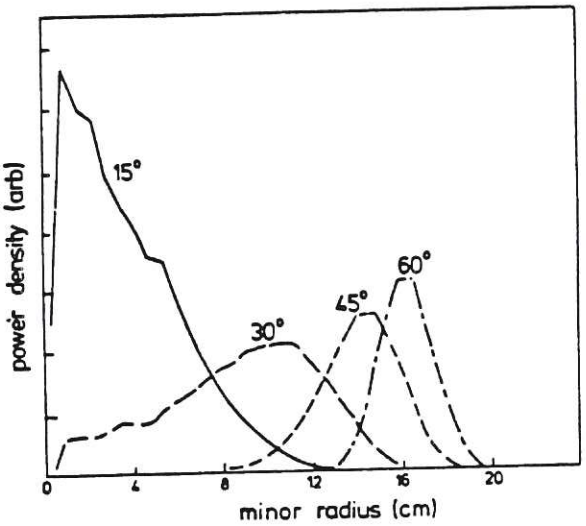

Fig.2 Profile of power absorption per unit volume as a function of launch angle for $\omega = \omega_{ce}$ at $R = R_o$ $n_{eo} = 4\times10^{19}m^{-3}$, $T_{eo} = 3keV$. The peak of the deposition profile moves out at high density mainly due to refraction.

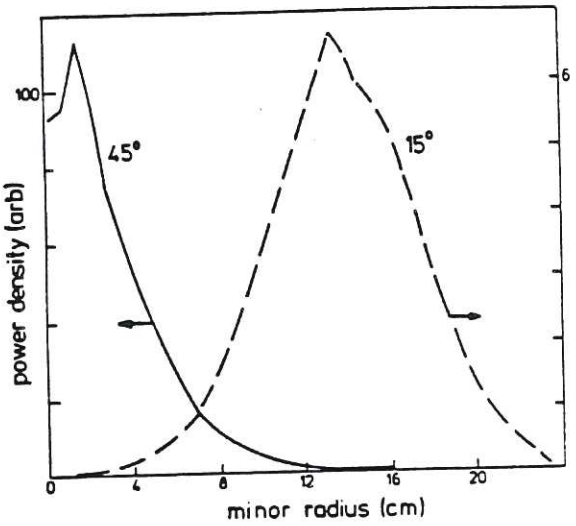

Fig.3 Profile of power absorption per unit volume at $\phi = 15°$ and $45°$ for $\omega = \omega_{ce}$ at $R = R_o + a/2$, $n_{eo} = 4\times10^{19}m^{-3}$, $T_{eo} = 3keV$. The central absorption efficiency is ~ 100% at $\phi = 45°$ due to Doppler resonance at high $k_{\parallel}$.

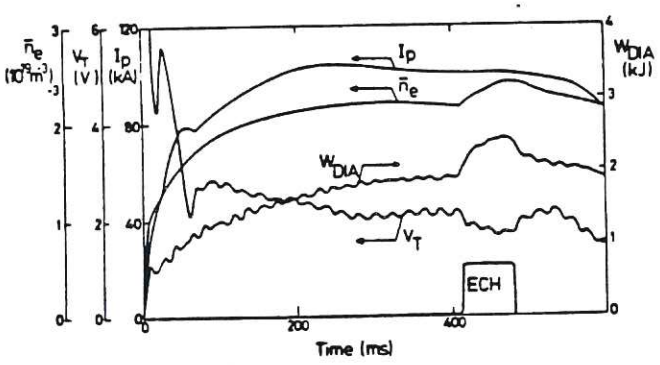

Fig.4 Traces of plasma current, I_p, density $\bar{n}_e$, energy content W_{DIA} (from diamagnetic measurements) and loop voltage V_T during a pulse with 100 to 150keV of ECRH heating at a toroidal field of 2.14T.

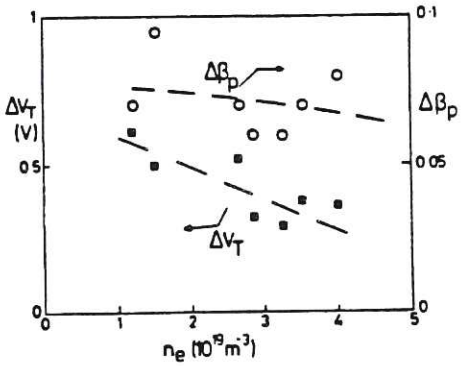

Fig.5 Variation with line-average density $\bar{n}_e$ of changes in diamagnetic beta, $\Delta\beta_p$, and loop voltage, ΔV_T, during heating with ECRH at a power level of 100 to 150kW in plasmas with $B_T = 2.14T$ and $I_p = 100kA$.

ECRH CURRENT DRIVE EXPERIMENTS ON CLEO

T Edlington, B Lloyd, M O'Brien, D C Robinson, T N Todd

Culham Laboratory, Abingdon, Oxon, OX14 3DB, UK
(UKAEA/Euratom Fusion Association)

Abstract A series of experiments to verify the existence of the RF driven current have been conducted. 28 GHz and 60 GHz gyrotrons have been used to study ECRH current drive in collisionality regimes with $\nu_* \sim 0.01 \rightarrow 0.1$. The experimental current drive efficiency has been compared with theoretical predictions. The sawtooth activity is influenced by the heating and current drive. The bootstrap current, which should be large in these hot electron plasmas, appears to be negligible.

Introduction Recent experiments [1] at both 28 and 60 GHz have used Vlasov antennae. Full power tests into free space with the 60 GHz antenna show a single crescent-shaped lobe 20° away from the axis of the waveguide, symmetrically distributed about the midplane at 70° to the direction of the toroidal field. The 28 GHz antenna launches waves at 53° with respect to the toroidal field. During the ECRH the plasma current is held constant by a fast feedback amplifier and the presence of any RF driven component of the plasma current can be deduced by observing differences in loop voltage when the plasma current is reversed with respect to the wave direction. Experiments were carried out both by reversing the plasma current and by reversing the wave launch direction, ie rotating the antenna.

Experimental results A clear and consistent difference in loop voltage, Fig 1, was observed in the 60 GHz experiment whether the current or antenna direction was changed, indicating a radio frequency current drive efficiency of ~ 30 A/kW. Up to aproximately 50% of the plasma current was driven in this way. The inferred driven current was found to scale

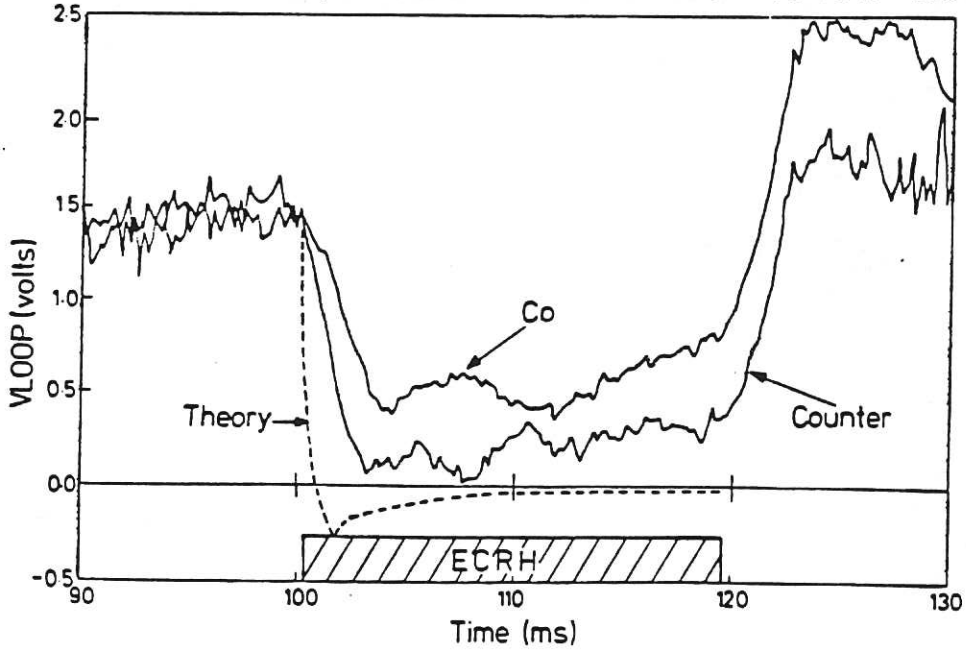

Fig 1. Loop voltage for clockwise and counter-clockwise plasma currents and the calculated voltage including the bootstrap current for the counter case. I_p=10kA, $\bar{n}_e$=3.5x10^{18}m^{-3}, T_{eo}=1.3 keV.

linearly with plasma current in the range 5 - 15 kA, and was maximised by having the resonance position somewhat inside the magnetic axis of the plasma. With the resonance at larger major radii both the absorption efficiency and current drive efficiency decrease, an effect probably associated with the increasing importance of the trapped electron population. Previous experiments at 28 GHz with $\nu_* \sim 0.01$ with large launch angles ($\sim 80°$) showed no evidence of RF current drive [2]. These experiments were repeated using the Vlasov antenna described above and again no discernible differences in the loop voltage behaviour were observed.

Theoretical modelling

Detailed ray tracing studies including calculations for current drive efficiency allowing for trapped particle effects have been undertaken to simulate the experimental conditions. These accurately reproduce the high absorption efficiencies and the scaling of the driven current with resonance position seen in the 60 GHz experiments with $\nu_* \sim 0.1$. However the predicted current is typically a factor of 3 larger than that observed. Possible reasons for this discrepancy include: enhanced trapped electron population, non-linear effects in the radio frequency field, distortion of the distribution function and asymmetric loss of fast electrons. Current drive relies on collisional slowing down (τ_s) of resonant electrons, which being close to the thermal population (in contrast to LHCD) may be susceptible to anomalous transport processes. If this timescale ($\sim \tau_E$) is comparable to or less than the collision times for the resonant electrons then the current drive may be partly or wholly disabled. In the 60 GHz experiments $\tau_s \lesssim \tau_E$ whereas at 28 GHz $\tau_s > \tau_E$. The absence of current drive in the 28 GHz experiments may be linked to this and to the more collisionless behaviour ($\nu_* \sim 0.01$) where clear enhancement of the trapped electron population is observed. Although the slowing down time of the trapped population appears to be classical, the distorted distribution function and the large step size of some of the particles in the radio frequency field may be such as to upset the current drive process.

Sawtooth activity

The calculated absorption and current drive profiles for a displaced plasma are shown in Fig 2 and are broader than the high q ohmic profiles. Together with the possible existence of a bootstrap current, this would be expected to lead to sawtooth suppression.

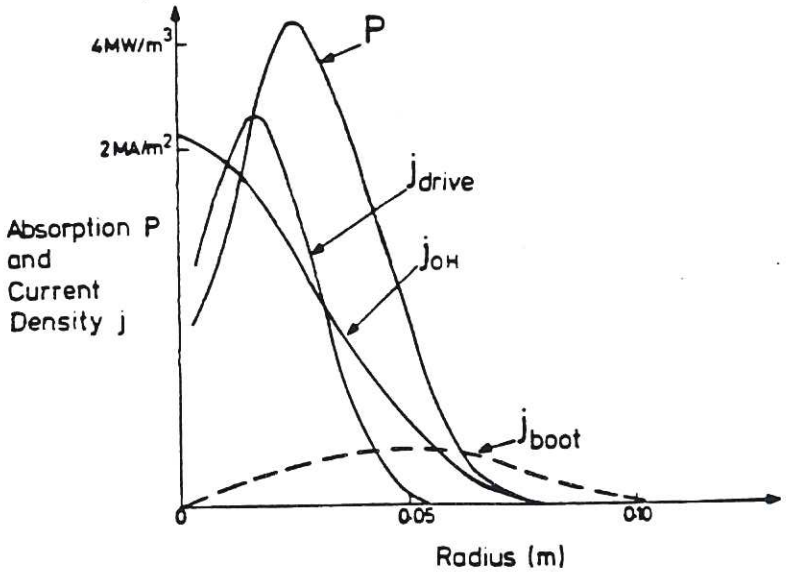

Fig 2 Predicted absorption, current drive, ohmic and bootstrap current profiles.

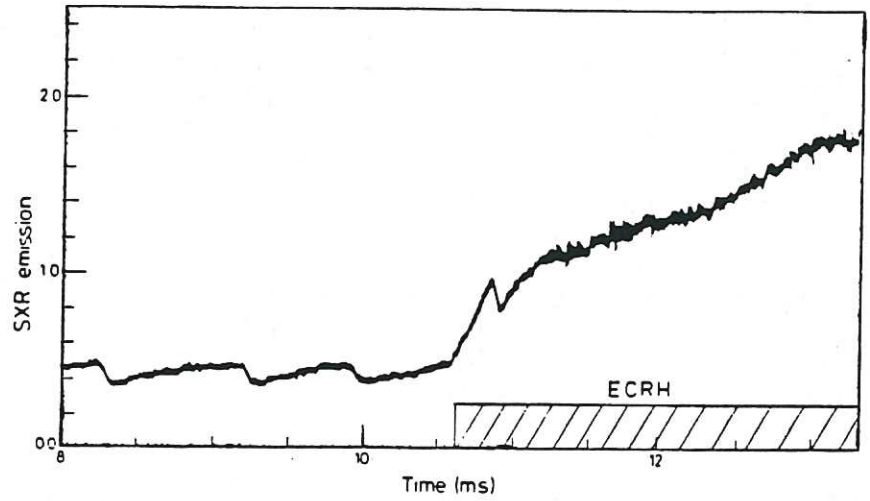

Fig 3a Sawtooth suppression at early heating times.

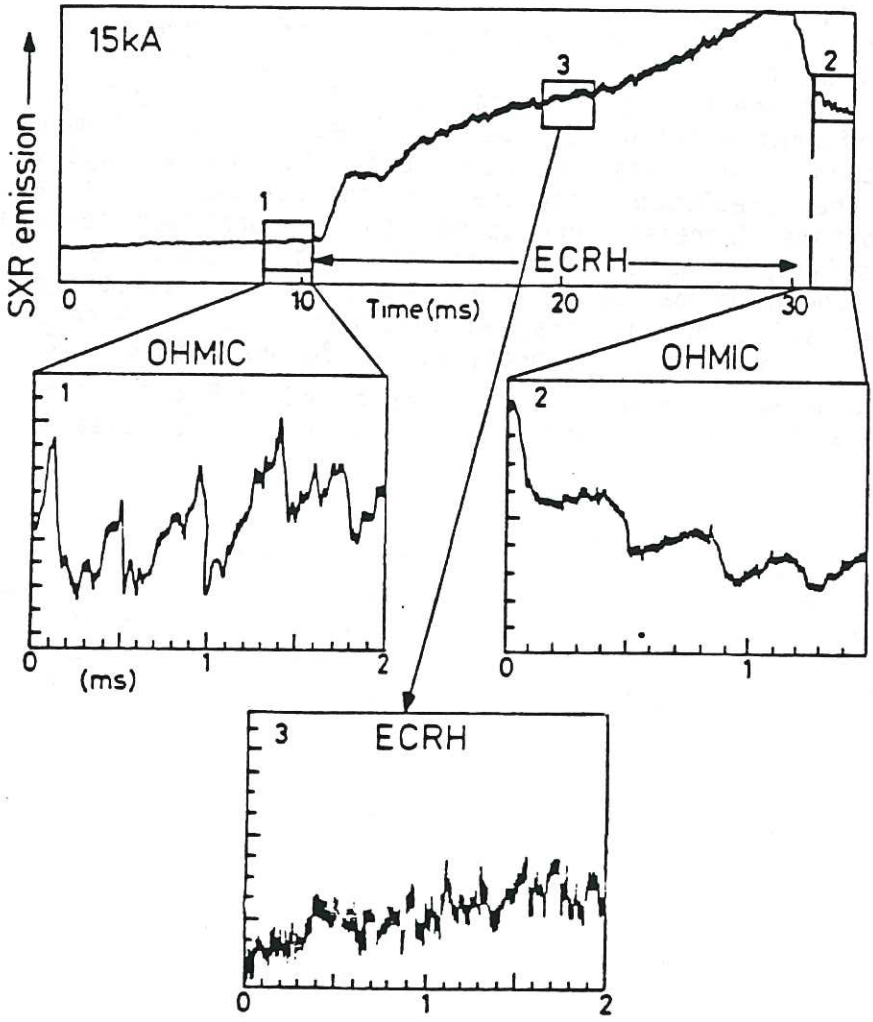

Fig 3b Sawtooth stabilisation and reappearance after ECRH.

Figure 3a shows that the sawtooth activity disappears shortly after the onset of the ECRH. The activity may reappear in the form of rounded sawteeth several ms later. As shown in Fig 3b the sawtooth activity recommences on switch-off of the ECRH. The sawtooth period is typically between 0.5 and 1 ms, $\sim \tau_E/2$, but this increases to over 2 ms when the resonance position is displaced outwards by 4 cm, ie close to the shifted magnetic axis. The sawtooth activity appearsto be more sensitive to the absorption profile and its location rather than the current drive profile. Current diffusion calculations for these profiles indicate that the central q value would change by 0.4 between co and counter current drive and yet no significant difference in sawtooth activity is observed. The increase in the sawtooth period to 2 ms if the resonance is displaced outwards is probably associated with the deposition profile being centered accurately inside the q=1 surface which is known to increase the period. As at 28 GHz no slow precursor activity is apparent before the sawtooth crash.

Bootstrap current

For these hot electron plasmas with $\nu^* \sim 0.1$ over most of the plasma profile and β_p values up to 3, the bootstrap current is calculated from the measured temperature, density, β_p, inferred profiles and assuming $T_i \ll T_e$, to be between 4 and 7 kA. This hollow profile bootstrap current, peaked at a radius $\lesssim$ 5 cm from the magnetic axis (Fig 2) should not only suppress sawtooth activity in these high q discharges but also initially depress the loop voltage significantly below zero as indicated in Fig 1 from current diffusion calculations. No transient decrease in the loop voltage is seen associated with the predicted decrease in inductance. The average symmetric loop voltage decrease corresponds to the observed temperature rise if the resistivity remains neo-classical. It is possible that the bootstrap current could be masked by enhancement in the resistivity from the neo- classical value due to trapped electron effects, although the transient behaviour should still be present. At 28 GHz with $\nu^* \sim 0.01$, $\beta_p \sim 5$, V_L remains even more positive than that indicated in Fig 1 and again no sawtooth stabilisation is observed, though a transient decrease in V_L is sometimes observed.

Conclusions

ECRH current drive experiments at 60 GHz with $\nu* \sim 0.1$ indicate a current drive efficiency about 3 times less than that predicted theoretically. Anomalous confinement of the electrons may account for this discrepancy. Transient sawtooth stabilisation is observed. These hot electron plasmas with high poloidal β do not provide any evidence for the bootstrap current.

Acknowledgement

We would like to thank the CLEO and ECRH teams for their support in this work.

References

[1] D C Robinson, IAEA Kyoto, paper CN-47/F-III-2, 1986
[2] T Edlington et al, Proc 13 EPS Conf Schliersee, Vol II, 219, 1986

Contribution to EPS, Madrid 1987

MHD STABILITY IN JET WITH PEAKED PRESSURE

T C Hender*, P S Haynes*, D C Robinson* and A Sykes*

JET Joint Undertaking, Abingdon, Oxon, OX14 3EA, UK
*Culham Laboratory, Abingdon, Oxon, OX14 3DB, UK.
(UKAEA/Euratom Fusion Association)

Introduction

A possible scenario to optimise the fusion product, for D-T operation in JET, is to have very peaked temperature ($T_0 \sim 16$keV) and density ($n_0 \sim 2 \times 10^{20} m^{-3}$) profiles, within a central ($q \sim 1$) low shear region [1]. This scenario is compatible with degraded confinement associated with powerful heating. To optimise the L-mode confinement time for this case a high current I = 7MA (at $B_T = 3.5T$) is proposed. At this current it is necessary to reduce the structural stresses by operating at an elongation $b/a \sim 1.7$, to closely align the flux surfaces with respect to the T F coils. The envisaged parameters for this case have a high central β to maximise the fusion product $\beta_0 \sim 20\%$. The corresponding $\langle\beta\rangle \sim 3\%$ is well below the Troyon limit of 4.5% [2]. The Troyon limit however is based on optimising with respect to relatively broad pressure profiles. In this paper we investigate the effect on ideal and resistive MHD stability of constraining the pressure profile to be peaked.

Intermediate and low n internal modes

In low shear regions a class of intermediate-n pressure gradient driven instabilities can exist [3]; these are sometimes called infernal modes. These modes, unlike the ballooning modes, have only one resonance within the radial extent of the mode and are thus sensitive to the radial location of the resonance. Figure 1 shows the growth rate (in poloidal Alfven units) as function of central q_0 for the n=3,4 and 5 infernal modes when $q = q_0 (1 + (r/0.71)^{12})^{1/6}$, $\beta_0 = 12\%$ and $P \propto \psi^4$

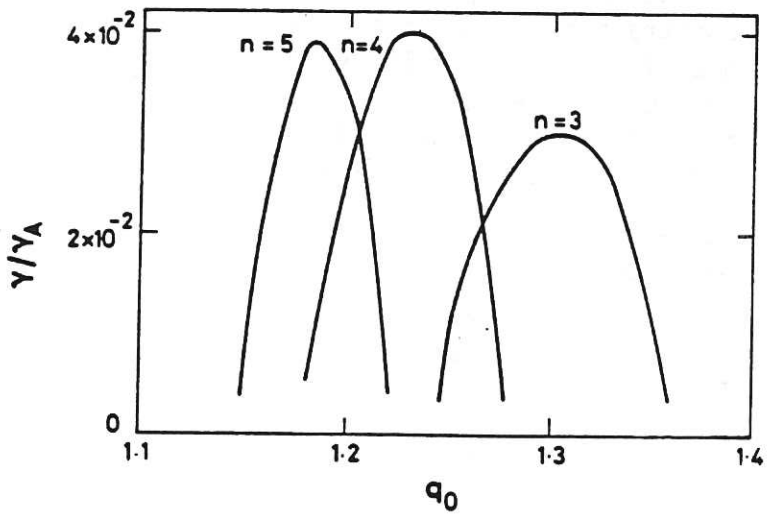

Fig 1 Growth rate of infernal modes (γ) v q_0

(ψ being the equilibrium poloidal flux). These parameters give a very flat central q and a peaked pressure profile. The equilibria have JET aspect ratio but a circular boundary has been used (because of computer memory limitations). Preliminary studies show that the results do not change significantly with ellipticity for b/a < 1.4. As expected the infernal mode stability is sensitive to the radial location of the resonance (ie q_0) and for example the n=4 (predominantly m=5) mode growth rate peaks near q_0 = 1.25. The results shown in Fig 1 are from a fixed boundary code but since these are radially localised internal modes their stability is insensitive to the wall location. For the n=4 mode we find a critical β_0 = 8%. For the case shown in Fig 1 the entire region between q_0 = 1.15 and 1.35 is unstable to the n=3, 4 or 5 mode. By considering higher n (> 6) this domain of instability can be extended closer to q_0 = 1. Also near q_0 = 1 the n=1 low shear internal kink modes (which have been proposed as an explanation for JET sawteeth [4]) are unstable. For the parameters envisaged in the D-T operation scenario [1] the requirement for stability to these modes is $q_0 \gtrsim 1.1$. Thus there is no reasonable value of q_0 for which stability to the n=1 and infernal modes occur when a low shear core and peaked pressure profile ($\beta_0 \gtrsim 10\%$) are considered.

Ballooning, Mercier and External Kink Modes

The conditions which are most detrimental for the infernal modes (ie low shear in the core and high pressure gradient) are optimal for the ballooning modes [5]; under these conditions relatively easy access to the second ballooning mode stable regime occurs. If however we increase the shear in the core (to improve the infernal mode stability) then access to the second stable region becomes much more difficult.

Figure 2 shows the effect on JET β-limits of constraining the pressure profile to be relatively peaked ($P \propto \psi^4$). The parameters for this study are I = 7MA, B_T = 3.5T and b/a = 1.68 and the equilibria are specified by $P' = a\psi^3$ and $FF' = \psi - a\psi^3 + b\psi^4$ (where $F = RB_T$). Comparing with a study by Sauremann [2] for identical parameters but broader pressure profiles ($P\alpha\ \psi^2 + a\psi^3$) shows the peaking has caused <β> to decrease from 4.7 to 2.7%. We have tried several other FF'

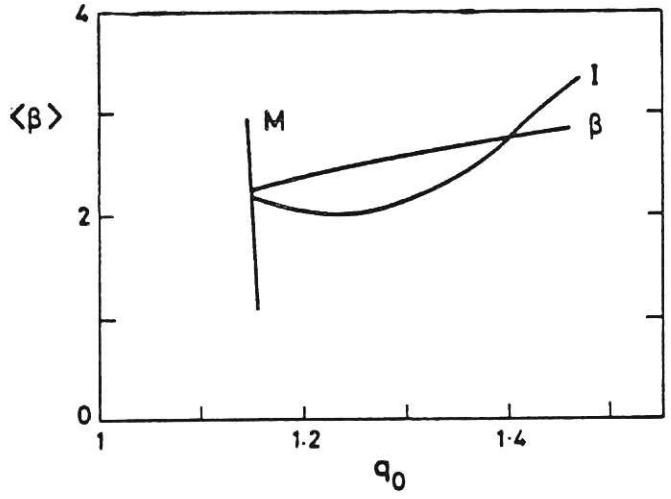

Fig 2 Mercier (M), Ballooning (B) and Kink mode (I) stability boundaries for Pα ψ^4

parameterisations in an attempt to improve the β-limits of the peaked pressure profile cases; for profiles which have moderate shear in the core region we have not been able to significantly improve the β-limit.

To make a systematic study of the effect of peaking the pressure profile on the β-limit, we have used a code which optimises the ballooning mode stability on each flux surface. Normally the optimisation criterion is to make the ballooning modes marginally unstable on every flux surface. However, by making the ballooning modes increasingly stable on the outer flux surfaces the pressure profile is correspondingly peaked. Figure 3 shows how $\langle\beta\rangle$ and β_0 vary as the peaking of the pressure profile ($P_0/\langle P\rangle$) is varied using this technique for a moderately sheared q-profile with $1.2 \leq q \leq 3.6$. The fully optimised case, ie ballooning modes marginally stable on every flux surface, corresponds to a peaking $P_0/\langle P\rangle = 3.2$. Thus in this case by increasing the peaking beyond 3.2 the critical $\langle\beta\rangle$ must decrease; but what is not so obvious is that β_0 should also decrease. This is a rather disappointing result since we are attempting to optimise the fusion product by maximising P_0.

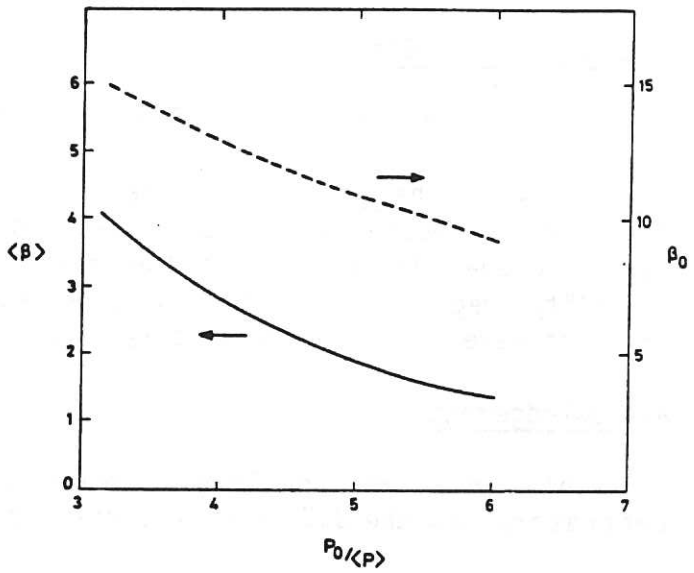

Fig 3 Decrease in critical $\langle\beta\rangle$ and $\langle\beta_o\rangle$ as pressure peaking is raised

Thus with I = 7 MA and B_T = 3.5 T it does not appear possible to achieve the required β_0 (~20%) in the first ballooning mode stability regime. We have, however, been able to increase the β_0 limit by reducing B_T. For B_T = 2.5T the first stability ballooning β-limit improves (α $1/B_T$) and for $q_0 \gtrsim 1.6$ direct access to second stability appears possible (even for peaked pressure profiles). However since $P_\alpha \sim \beta^2 B^4$ we have not been able to achieve a sufficient increase in β, by reducing B_T, to raise the alpha power. We have had more success in improving the ballooning β-limits, for moderately sheared cases, by going to rather broad pressure profiles. For example for I = 7MA, B_T = 3.5T and b/a = 1.68 we have been able to achieve second stability with $\beta_0 \gtrsim 30\%$ by using the broad profiles $P \alpha \phi^{1.4} + a\,\phi^{2.5}$.

Resistive Stability

Here we are mainly interested in the n = 1 and 2 resistive tearing modes which are associated with the major disruption. These are generally stabilised by average curvature effects in JET [6] but for the peaked pressure profiles this effect is weaker since the local pressure gradient at q = 2 (and $^3/_2$) is smaller. However for the relatively rounded q-profile, peaked pressure cases ($P \alpha \psi^4$) of Fig.2 we still find complete tearing stability for $S \gtrsim 10^7$. (Here S is the magnetic Reynolds number $\sim 10^8$ for JET). However as the q-profile is flattened (and the current profile is broadened) so the tearing modes are increasingly destabilised.

Conclusions and Discussions

For I = 7MA and b/a = 1.7 we find that the main ideal instabilities (ballooning, n = 1 kink and infernal modes) impose a limiting central $\beta \lesssim 10\%$ when the pressure is relatively peaked ($P \sim \psi^4$); this leads to a factor of 4 reduction in the α power compared with that envisaged in ref [1]. However if we broaden the pressure profile then access to second stability regime is relatively easy and $\beta_0 > 30\%$ is possible. Such profiles have Q > 1 and require $\tau_E \lesssim 1$s.

Acknowledgement

This work was performed under a task agreement between Culham Laboratory and the JET Joint Undertaking.

References

[1] P H Rebut et al, paper A-I-2 IAEA Kyoto (1986)
[2] H Saurenmann et al, Lausanne report LRP 263/85
[3] R J Hastie et al, Nucl Fusion 21 (81) 187
[4] J A Wesson, Plasma Phys 28 (86) 243
[5] S Seki et al, Nucl Fusion 27 (87) 331
[6] T C Hender et al, paper A-V-3 IAEA Kyoto (1986)

Contribution to EPS Madrid, 1987

MHD STABILITY IN TOKAMAKS WITH LOW CENTRAL q

T C Hender, R J Hastie and D C Robinson

Culham Laboratory, Abingdon, Oxon, OX14 3DB
(UKAEA/Euratom Fusion Association)

Introduction

Measurements on TEXTOR have shown that the central q_0 can be as low as 0.6 [1]. These measurements also suggest that the current (and hence q) has a reduced gradient near q=1. In this paper we study the effect on stability of reducing q' near q=1 using the fully toroidal resistive MHD code FAR [2]. The results given may also be interpreted as showing the effect of local reductions in the current gradient near q=1 from RF current drive/heating.

q'≠0 at q=1

First we shall study the effect of reduced, but finite, shear near q=1. In this case the analytic theory given in [3] is applicable. When $q_a < 2$ the result is

$$\frac{1}{\Delta_1'} + \frac{2}{\pi}\sqrt{\left(\frac{r_1}{q'}\right)}\left[\frac{3\gamma}{S}\right]^{\frac{1}{4}} \frac{\mu-1}{\mu} \frac{\Gamma\left(\frac{\mu+5}{4}\right)}{\Gamma\left(\frac{\mu+3}{4}\right)} = 0 \qquad (1)$$

where r_1 is the q=1 radius, γ is the n=1 growth rate normalised to the poloidal Alfven time, S is the magnetic Reynolds number and $\mu = \sqrt{3}\gamma^{3/2}S^{1/2}/(r_1 q')$. The driving energy from the region external to q = 1 (Δ_1') is related to the toroidal potential energy (δW_T) by [4]

$$r_1\Delta_1' = \frac{(r_1 q'(R/r_1))^2}{\delta W_T} \qquad (2)$$

Since δW_T is independent of aspect ratio and relatively insensitive to local variation in q', we see that reducing the shear at q = 1 and/or the aspect ratio has a stabilising effect (ie, reduces Δ_1'). When Δ_1' is relatively small ($\lesssim 50$) and typical values for S($\gtrsim 10^6$) are assumed, then $\mu \ll 1$ and Eq (1) reduces to the normal tearing mode dispersion relation with $\gamma \propto S^{-3/5}$. Figure 1 shows how the n=1 growth rate (γ) varies with aspect ratio (A), and compares γ computed from Eqs (1) and (2) with results from the FAR code. In this case β_0 = 0%, S = 10^9 and q = $0.7+1.2r^2-0.72(r^2-0.25)\,e^{-100(r^2-0.25)^2}$ [the exponential term reduces q_1' by 60%]. From

Fig.1 it is clear at the larger aspect ratios [where the ordering assumption used in deriving Eqs (1) and (2) are valid] that the analytic and numerical results are in good agreement. However, as the aspect ratio is decreased higher order corrections give an additional stabilising effect and $\gamma \sim 0$ by A = 2.5. For A<2.5 the FAR code suggests the solutions are damped and stable; this is however difficult to establish conclusively with an initial value code. The high value of $S (= 10^9)$ used in these calculations was chosen to allow us to use the simple tearing mode limit of Eq(1) for calculating the analytic growth rates (even at larger A). It is important to note that the stabilisation is not caused by this high value of S, and that the critical A at which $\gamma \sim 0$ is insensitive to S.

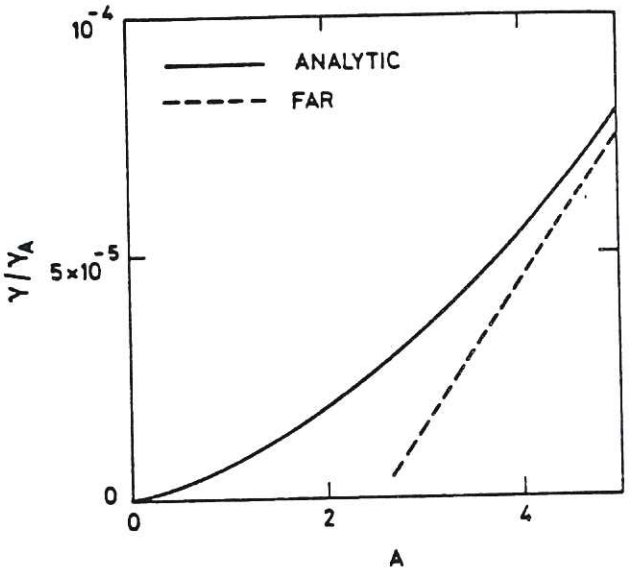

Fig 1. Growth rate (γ) v Aspect Ratio (A) comparing analytic theory [Eq (1) and (2)] with numerical FAR results

The effect of β on these results is mainly determined by the β-dependence of δW_T (and hence of Δ_1'). The relevant definition of β which enters δW_T is [3]

$$\beta_B = - \frac{2}{B_\theta^2} \int_0^{r_1} \frac{\partial P}{\partial r} \left(\frac{r}{r_1}\right)^2 dr \qquad (3)$$

As β_B is raised the value of δW_T decreases, as marginal stability is approached, and thus Δ_1' ($\alpha 1/\delta W_T$) increases. Hence raising β_B has a destabilising effect. Figure 2 confirms this by plotting the growth rate (γ) as a function of β_B for several pressure profiles. The q-profile in this case is the same as Fig. 1, $S = 10^6$ and A = 4. The close agreement between the growth rates for the 3 pressure profiles shown in Fig. 2 also confirms that β_B is the appropriate definition of β in determining the stability properties. Since β_B is determined from the pressure gradient (and not the pressure), in a device such as TEXTOR where the n and T profiles tend to be relatively broad and flat within q = 1, there should be little effect due to β (ie, $\beta_B \simeq 0$).

We have also examined the effects of local flattenings in the pressure profile near q = 1. At q = 1 the average curvature effect is very weak and determined by a term related to the Shafranov shift [2]. Numerically we find that locally flattening P near q = 1 has a slight destabilising effect, which is as expected since we are removing a small stabilising effect due to the average curvature (D_R < 0, when dP/dr < 0 at q = 1).

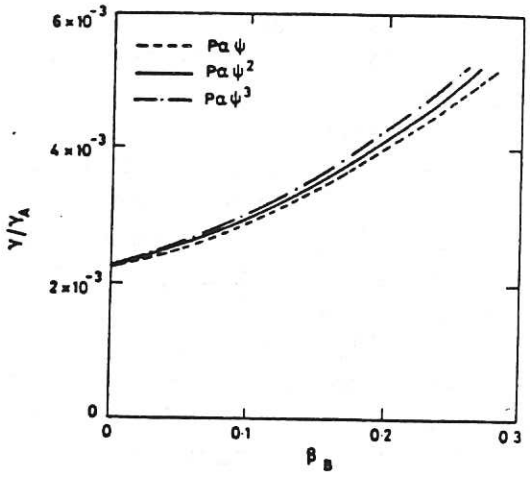

Fig 2. γ *v* β_B *for various profiles*

We have so far considered profiles with q_a < 2. For q_a > 2 a coupling occurs between the q = 1 and 2 surfaces; as noted in [3] this coupling is particularly strong for cases such as we are studying with reduced shear at q = 1. At β=0 this coupling with the m=2 eigenmode is destabilising (irrespective of the sign of Δ_2'). At finite-β, there may be a strong average curvature stabilisation at the q=2 surface but we have not yet investigated the effect of this on the m=1 stability. Numerically, at β=0 we have studied the profile $q = 0.6+3.2r^2-1.9(r^2-0.125)e^{-100(r^2-0.125)^2}$, which has q_a = 3.8. In this case there is still a stabilising effect as A is reduced but we have not been able to achieve complete stability for A $\geq$ 2.

We have also studied the effect of varying q_0. Raising q_0 decreases δW_T and thus if Rq_1' is held constant, Δ_1' increases [cf Eq (2)]. We have verified this destabilisation numerically by studying the profile $q = 0.85 + 1.1r^2 - 0.45(r^2 - 0.136)e^{-100(r^2 - 0.136)^2}$ (which has the same Rq_1' as the profile used in Fig 1). Again there is a stabilising effect as the aspect ratio is reduced but complete stability is not achieved for A > 2.

As the m=1 mode is stabilised by decreasing A, the flows associated with the instability become localised to the region near q = 1. Thus we should expect in the initial precursor phase of the sawtooth that the activity will be localised near q = 1 for this type of q-profile. Also this localisation makes additional stabilisation from kinetic effects likely.

q' = 0 at q = 1

We now consider the extreme case of a point of inflection at q = 1. There is still a strong stabilising effect as the aspect ratio is reduced. Figure 3 shows the growth rate as a function of aspect ratio for $q = 0.6 + 2.2r^2 - 2.2(r^2 - 0.43^2)\, e^{-\alpha(r^2-0.43^2)^2}$, β_0 = 0% and S = 10^5. The stabilising effect increases as the region of flattening is increased (ie, α decreased). Also shown in Fig.3, for reference, are unflattened q-profile results (with γ reduced by 2). For the unflattened case there is

no significant stabilisation as the aspect ratio is reduced; the slight reduction in growth rate (for $A \lesssim 4$) occurs because the mode switches from the aspect ratio independent resistive interchange mode ($\gamma \propto S^{-1/3}$) to the aspect ratio dependent tearing mode ($\gamma \propto S^{-3/5}$) as A is decreased (c.f Eqs (1),(2) and Ref [4]). In contrast to the $q' \neq 0$ cases, the growth rate becomes overstable when the strong stabilisation occurs at small aspect ratio in these point of inflection cases. Such overstable behaviour is indicative of an effect arising from the properties of the MHD equation within the resistive layer about $q = 1$. Further confirmation of this arises from the fact that the critical aspect ratio at which the strong stabilisation occurs can be increased by raising S, for the point of inflection cases (but not for the $q' \neq 0$ cases); even for $A \sim 10$ strong stabilisation can be achieved for $S \gtrsim 2 \times 10^6$. Even though this stabilisation occurs at relatively large aspect ratio it remains a purely toroidal phenomena (as are all the stabilisation effects discussed in this paper). This is because in cylindrical geometry the m = 1 mode is ideally unstable (even at $\beta = 0$) and has a growth rate which increases like $A^{-6/5}$ for the point of inflection case (A^{-2} for $q' \neq 0$ case).

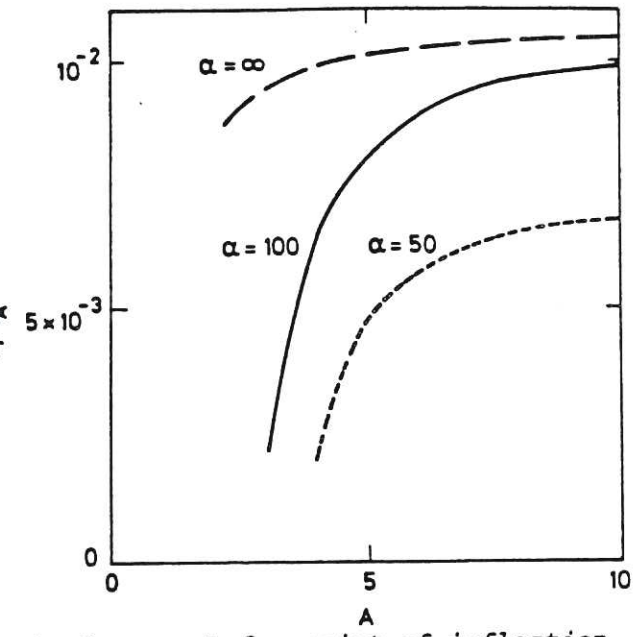

Fig 3. γ v A for point of inflection q-profile. Also shown for reference is unflattened ($\alpha = \infty$) result (γ x 0.5)

Conclusion and Discussion

For cases with reduced, but finite shear at $q = 1$ analytic theory predicts $\gamma \propto q_1'^2 A^{8/5}$; numerically we find an even stronger stabilisation as A is reduced with complete stability below some A_{crit} (~ 3). The exact value of A_{crit} is profile dependent and for example increases as the shear at $q = 1$ is decreased. The effects of β are destabilising but in a device such as TEXTOR where the pressure gradients tend to be small within $q = 1$ the effect is weak. As q_a is raised complete stabilisation by reducing A becomes harder to achieve. In the extreme case where there is a point of inflection in the q-profile at $q = 1$ an additional stabilisation arises from the properties of the MHD equations within the $q = 1$ resistive layer; this layer stabilising effect becomes stronger at higher S.

References

[1] H Soltwisch et al, IAEA Kyoto paper A-V-1-31 (1986)
[2] T C Hender et al, Culham Lab report, CLM-P794 (1986)
[3] M N Bussac et al, IAEA Berchtesgaden, Vol 1 (1977) 607.
[4] R J Hastie et al, Culham Lab report, CLM-P801 (1987)